Engineering Chemistry
ISSN: 2813-6535, Vol. 13, pp 39-50
doi:10.4028/p-9bwDd3

Submitted: 2025-08-19
Revised: 2025-10-31
Accepted: 2025-11-03
Online: 2026-02-18

Enhanced Humidity Sensing Properties of Sn-Doped ZnO Nanostructures on AZO/PET Substrates via Sol-Gel Immersion Method

Shahirah Ahmad Kamal[1,a], Nor Diyana Md Sin[2,b*], Mohamad Hafiz Mamat[2,c], Mohamad Zhafran Hussin[2,d], Fatimah Khairiah Abd Hamid[2,e], Mohd Hanapiah Abdullah[3,f] and Noor Asnida Asli[4,g]

[1]NANO-ElecTronic Centre (NET), Universiti Teknologi MARA (UiTM) Selangor, 40450 Shah Alam, Selangor, Malaysia

[2]Faculty of Electrical Engineering, Universiti Teknologi MARA, Cawangan Johor Kampus Pasir Gudang, 81750 Masai, Johor, Malaysia

[3]Faculty of Electrical Engineering, Universiti Teknologi MARA, Cawangan Pulau Pinang, 13500 Permatang Pauh, Pulau Pinang, Malaysia

[4]NANO-SciTech Lab, Functional Materials and Nanotechnology Centre, Institute of Science, Universiti Teknologi MARA, 40450 Shah Alam, Selangor, Malaysia

[a]shahirahsak@gmail.com, [b*]diyana0366@uitm.edu.my, [c]mhmamat@uitm.edu.my, [d]mzhafran@uitm.edu.my, [e]fatimahkhairiah@uitm.edu.my, [f]hanapiah801@uitm.edu.my, [g]asnida1462@uitm.edu.my

Keywords: Doped ZnO, Nanostructure thin film, Low Temperature synthesis, Humidity sensor, Flexible sensor.

Abstract. This work reports the structural and humidity-sensing properties of Tin (Sn)-doped Zinc Oxide (ZnO) nanostructures deposited on Aluminum-doped Zinc Oxide/Polyethylene Terephthalate (AZO/PET) substrates via the sol-gel immersion method. Accordingly, X-ray Diffraction (XRD) and FESEM analyses confirmed that low-level Sn incorporation (1 at.%) enhanced the (002) orientation and crystallinity, while higher doping introduced lattice distortion and defects. Meanwhile, humidity sensing measurements revealed that undoped ZnO exhibited the highest sensitivity (178.5), though it recorded a very slow response (231 s) and recovery (648 s). In contrast, 1 at.% Sn-doped ZnO achieved a balanced performance, combining high sensitivity (144.4) with much faster response (121 s) and recovery (411 s). These results demonstrate that controlled Sn doping optimizes ZnO nanostructures for flexible humidity-sensing applications. Overall, the findings provide valuable insight for developing real-time environmental and wearable sensing devices, with future work focusing on stability testing and mechanical flexibility evaluation.

Introduction

Humidity sensors are measuring devices that determine the moisture content, or Relative Humidity (RH%), in the atmosphere and play a significant role across various industrial sectors and applications. The recent improvements in humidity sensors have expanded the market for humidity sensors across numerous industries, such as semiconductors, agriculture, and medicine [1,2]. For instance, the semiconductor industry precisely regulates humidity levels during wafer processing using humidity sensors [3,4]. Meanwhile, the agricultural sector employs humidity sensors to monitor soil moisture. In the context of the medical industry, humidity sensors are utilized to monitor human respiration through various tools, such as incubators, ventilators, and biological products.

An ideal humidity sensor should have key characteristics, such as minimal hysteresis, strong thermal stability, high sensitivity, fast response, and quick recovery. In this regard, metal oxide nanomaterials are used to fabricate high-performance humidity sensors due to their large specific surface areas [5]. In particular, Zinc Oxide (ZnO) has experienced a surge in popularity over the years, as it is among the most suitable metal oxide candidates for producing high-quality humidity sensors and other nanotechnology applications [5]. This includes electronics, ultraviolet, and photoconduction [4,6].

The extensive use of ZnO across various technical domains is attributed to its excellent properties, such as a wide bandgap (3.37 eV), an optimal excitation binding energy (60 meV), and the ability to form at low temperatures [6,7]. Notably, the ZnO surface contains numerous oxygen vacancies, which facilitate strong interactions between water molecules and the nanostructure, thereby enhancing humidity sensitivity [4]. On top of that, ZnO is naturally non-toxic and cost-effective.

In recent years, various synthesis and improvement methods for ZnO, for instance, sol-gel immersion [8], Radio Frequency (RF) magnetron sputtering [9], spin-coating [10], as well as Chemical Vapor Deposition (CVD)[11], have been implemented. Alternatively, the doping technique has been implemented to improve ZnO's humidity-sensing performance and enhance the surface area [12,13]. Notably, metal oxides commonly used as doping materials include Aluminum (Al), Copper (Cu), Indium (In), and Tin (Sn) [12,13]. Remarkably, the effectiveness of ZnO in humidity sensors is greatly affected by the choice and amount of dopant, along with its electrical characteristics [6,14].

Similar dopants have also been explored in other composite systems beyond ZnO-based structures. For instance, studies on ceramic composites demonstrated that Sn doping effectively enhanced structural stability and improved electrical properties [15]. Likewise, polymer-based composites incorporated with Sn dopants have exhibited improved dielectric behavior and conductivity, highlighting the versatility of this dopant across different material systems [16,17]. Collectively, these findings across ceramics, polymers, and other composites further emphasize the potential of Sn as a functional dopant, thereby justifying its application in ZnO-based humidity sensors.

Meanwhile, plastic-based substrates are rarely reported, though they are attracting greater attention from the research community due to their unique advantages over glass substrates. In particular, plastic-based substrates are lightweight, flexible, durable, and robust and consume minimal power in electronic devices [18,19,20, 9]. As such, Polyethylene Terephthalate (PET) is one of the most widely utilized plastic-based substrates in electronic device applications.

To the best of our knowledge, comprehensive studies on Sn-doped ZnO on PET substrates remain limited. Considering the potential use of such integration in humidity sensor development, this paper investigated the structural characteristics and humidity-sensing capabilities of a Sn-doped ZnO nanorod array-based PET substrate utilizing the sol-gel immersion method. In essence, the results of this research are projected to offer a detailed understanding of their structural properties, which are essential for advancing their use in future humidity-sensing technologies.

Methodology

The preparation of Aluminum-doped Zinc Oxide (AZO) seed layer solution involved dissolving 0.4 M Zinc Acetate Dihydrate ($Zn(CH_3CO_2)_2.2H_2O$, 99.5% purity, Aldrich) served as the precursor, 0.004 M Aluminum Nitrate Nonahydrate ($Al(NO_3)_3.9H_2O$, 98% purity, Analar) prepared as the dopant source, 0.4 M Monoethanolamine (MEA, $H_2NCH_2CH_2OH$, 99.5% purity, Aldrich) utilized as the stabilizer, and 2-methoxyethanol as the solvent. Subsequently, the mixture was stirred and heated on a hotplate stirrer at 80°C and 300 rpm for 3 h, then left to age at room temperature for 24 h at 300 rpm to obtain homogeneous solutions. Then, the mixed solution was applied to the PET substrate using the spin coating method, with ten drops deposited at 3,000 rpm for 60 s. The deposition process was repeated five times to obtain the desired thickness. Following this, the sample was dried at 80°C for 10 min between each spin coating prior to being annealed at 140°C for 1 h.

The Sn-doped ZnO sol-gel solution was prepared using 0.1 M Zinc Nitrate Hexahydrate ($Zn(NO_3)_2.6H_2O$, 98.5% purity, Schmidt) as the precursor, while 0.1 M Hexamethylenetetramine (HMT, $C_6H_{12}N_4$, 99% purity, Aldrich) served as the stabilizer. Both reagents were dissolved in 200 mL of Deionized Water (DIW) and gently stirred until the mixture turned a whitish color. The solution was then subjected to ultrasonication at 50°C for 30 min, followed by continuous stirring on a hotplate stirrer at 250 rpm for 3 h.

The deposition of a Sn-doped ZnO sol-gel solution onto the AZO seed layer was performed using an immersion technique. Initially, a sonicated solution was transferred into a Schott bottle containing the AZO seed-layer-coated PET substrate, which was then placed in a 95°C water bath for 30 min to promote growth. Following immersion, the samples were removed, rinsed with DI water to eliminate

residual particles, and subsequently dried and annealed at 80°C and 140°C, respectively. This procedure was repeated with varying immersion durations ranging from 1 to 4 h, different doping (Sn) concentration percentages, and different annealing times (80°C to 130°C) to obtain optimized characterization properties. For doped films, the process was repeated, and Sn (IV) chloride pentahydrate ($SnC_{l4}.H_2O$, 98%, Sigma Aldrich) was added to the mixture at doping concentrations of 1, 2, 3, 4, and 5 at.% Sn.

Characterization of Sn-doped ZnO thin film on an AZO seed layer was performed to assess its structural properties and sensor performance for humidity-sensing applications. Next, structural analysis of the samples was performed utilizing FESEM (JEOL JSM-7600F) and X-ray Diffraction (XRD, Rigaku Ultima IV). Accordingly, humidity sensor measurements were performed on the fabricated device, with Silver (Ag) as the metal contact deposited by thermal evaporation. The distance between the electrodes was 60 μm. Note that the metal contact served to effectively capture or transfer the signal from the thin film to the external circuit within the humidity chamber. In line with this, sensor performance was evaluated utilizing current-voltage measurements (I-V, Keithley 2400) and a humidity-sensing measurement system (ESPEC SH261). Concurrently, the sample was evaluated in a humidity chamber set at 25°C (room temperature), with RH% ranging from 40% to 90%.

I-V measurements were performed using a two-probe setup and the humidity sensor measurement system (ESPEC SH261). Note that a voltage ranging between -5 V and 5 V was provided using the Keithley 2400 instrument. A thermal evaporator was utilized to deposit an Ag layer onto the film. This Ag layer serves as a metal contact/electrode for the purpose of I-V characterization.

Correspondingly, the performance of the samples as sensors was evaluated through I-V measurements. These measurements aimed to assess how varying nanostructures influence the sensor's response time, recovery time, and sensitivity. In this study, sensitivity values were obtained from I-V data to assess the overall performance of the humidity sensor. Hence, the sensitivity can be written as below (Eq. 1) [21]:

$$S = \frac{I_{90}\ RH\%}{I_{40}\ RH\%}, \tag{1}$$

where

S = sensitivity,

$I_{40}RH\%$ = sensor's current under exposure to minimum humidity (40% RH), and

$I_{90}RH\%$ = sensor's current in the maximum humidity (90% RH).

In addition to sensitivity (S), a humidity sensor's performance is influenced by its response time (adsorption) and recovery time (desorption). The response time is the time required for the transient current to stabilize to 90% of the total resistance change when RH increases from 40% to 90%. Conversely, the recovery time corresponds to the change from high RH (90%) back to low RH (40%). These parameters are calculated employing (Eq. 2) and (Eq. 3) [23]:

$$I(t) = I_0\left(1 - exp\left(-\frac{t}{t_r}\right)\right), \tag{2}$$

Regarding the response time (adsorption process)

$$I(t) = I_0 exp\left(-\frac{t}{t_d}\right), \tag{3}$$

Concerning the recovery time (desorption process)

where
I = the magnitude of the current,
I_0 = the saturated current,
t = the time,
t_r = the response time constant, and
t_d = the recovery time constant.

Results and Discussion

Structural properties from Fig. 1 illustrate the surface morphology of ZnO nanostructures for (a) undoped and Sn-doped samples at (b) 1 at.%, (c) 2 at.%, (d) 3 at.%, (e) 4 at.%, and (f) 5 at.% prepared using the sol-gel immersion method. Note that the ZnO nanostructure was characterized and analyzed using FESEM at a 5 kV voltage and under 50,000x magnification. In addition, the figure displays nanostructures with a hexagonal structure. However, there is variation in the nanostructure diameter, possibly due to the non-uniform surface of the AZO seed layer deposited on PET substrates [24].

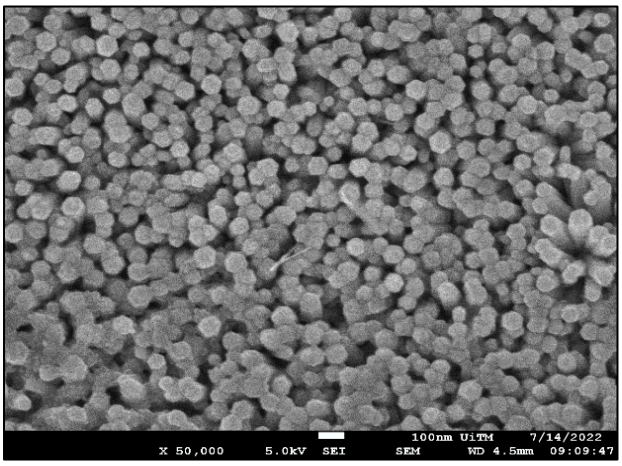

a) undoped

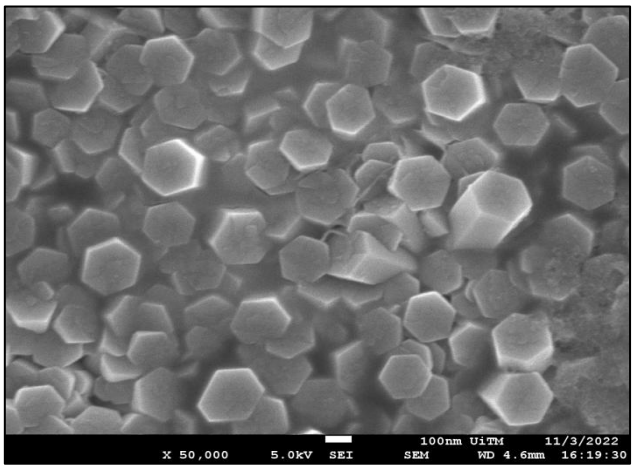

b) 1 at.%

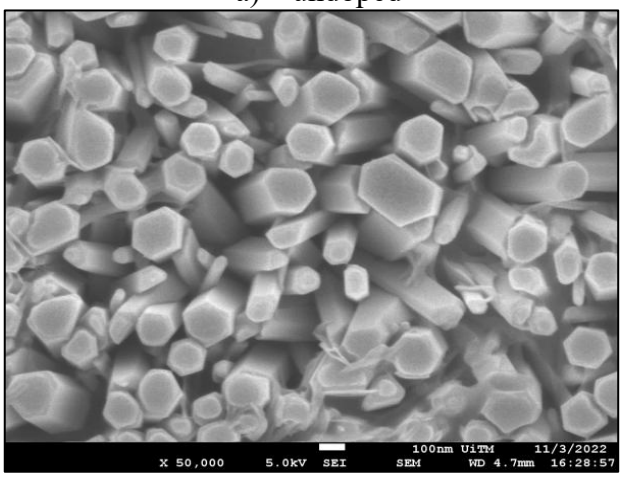

c) 2 at.%

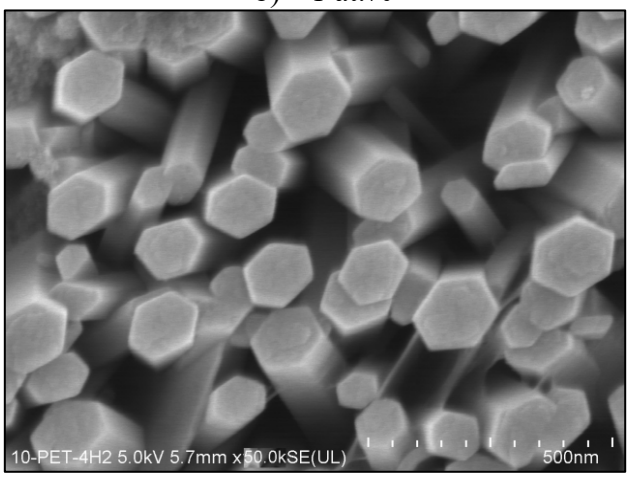

d) 3 at.%

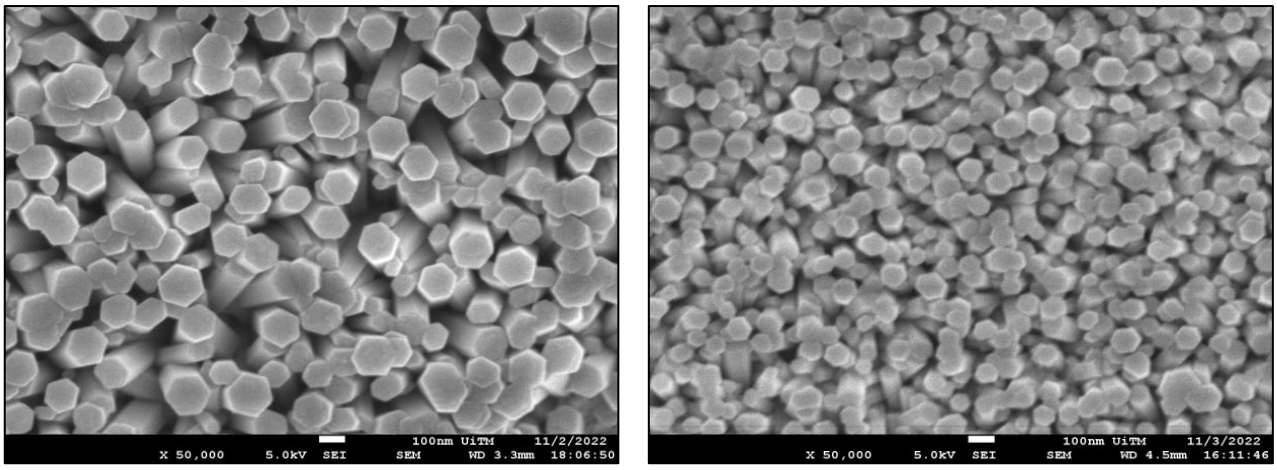

e) 4 at.% f) 5 at.%

Fig. 1 FESEM images of samples on different doping concentrations at.% Sn of (a) undoped, (b) 1 at.%, (c) 2 at.%, (d) 3 at.%, (e) 4 at.%, and (f) 5 at.%

The samples undergo different growth processes as the doping percentage increases. At 1 at.% doping (165 nm), the average diameter is significantly larger than in the undoped state (83 nm). As the doping concentration continues to rise to 2 at.% and 3 at.% Sn, the average diameter also experiences a further increase, reaching 217 nm and 231 nm, respectively. However, at 4 at.% doping, the average diameter decreases to 157 nm. This could be attributed to a complex interplay between doping-induced strain, surface energy effects, and crystallinity. Furthermore, it is possible that at higher doping concentrations, the growth kinetics are influenced by the interplay of these factors, leading to a different size distribution. At 5 at.% doping, the trend of decreasing average diameter continues, reaching 92 nm. This suggests that beyond a certain doping concentration, the incorporation of foreign atoms might hinder nanostructure growth, leading to smaller particle sizes. Previous research has argued that the average diameter decreases as the Sn doping concentration increases [25,26]. This behavior can be explained by the substitution of smaller Sn^{4+} ions (0.69 Å) into larger Zn^{2+} sites (0.74 Å), which introduces both an ionic-radius mismatch and a valence-state difference. Consequently, the size mismatch generates local lattice distortion, while the higher valence state of Sn^{4+} creates a charge imbalance, which is typically compensated by oxygen vacancies. Moreover, these effects combine to produce local strain within the ZnO lattice, thereby increasing lattice distortion and suppressing crystallite growth, consistent with our findings and previous reports [25,27]. In line with this, Ismail et al. have also stated that a doped ZnO crystal structure exhibits greater formation energy compared to undoped ZnO, indicating that the incorporation of Sn inevitably enhances lattice distortion during growth [25]. On the other hand, the observed increase in nanostructure diameter at higher dopant concentrations is attributed to enhanced coalescence and lateral growth. In contrast, the decrease in diameter is due to strain and charge imbalance caused by Sn incorporation. Table 1 below provides the recorded diameter.

Table 1. The average diameter of ZnO nanostructure with different doping concentrations at.% Sn

Doping at % Sn	Average Diameter [nm]
undoped	83
1	165
2	217
3	231
4	157
5	92

The samples' structural analysis was performed using XRD. Fig. 2 illustrates the XRD spectra of the Sn-doped ZnO nanostructure at various doping at.% Sn of (a) undoped, (b) 1 at.% (c) 2 at.%, (d) 3 at.%, (e) 4 at.%, and (f) 5 at.%, respectively. The patterns in Fig. 2 display characteristic diffraction

peaks consistent with the hexagonal wurzite structure of ZnO (JCPDS card no. 36-1451) and the tetragonal rutile structure of SnO_2 (JCPDS card no. 41-1445) at various doping concentrations [24, 28]. In this research, the XRD analysis identified specific diffraction peaks for SnO_2 at 2θ angles of ± 26.6°, ± 33.8°, and ± 37.9°, according to lattice planes (110), (101), and (200), respectively. For ZnO, primary diffraction peaks were observed at ± 31.8°, ± 34.4°, and ± 47.5°, in accordance with lattice planes (100), (002), and (101), respectively. Notably, the most prominent peak across all samples examined was the (002) reflection at 2θ = 34.5◦, which refers to the preferential c-axis orientation of ZnO nanorods.

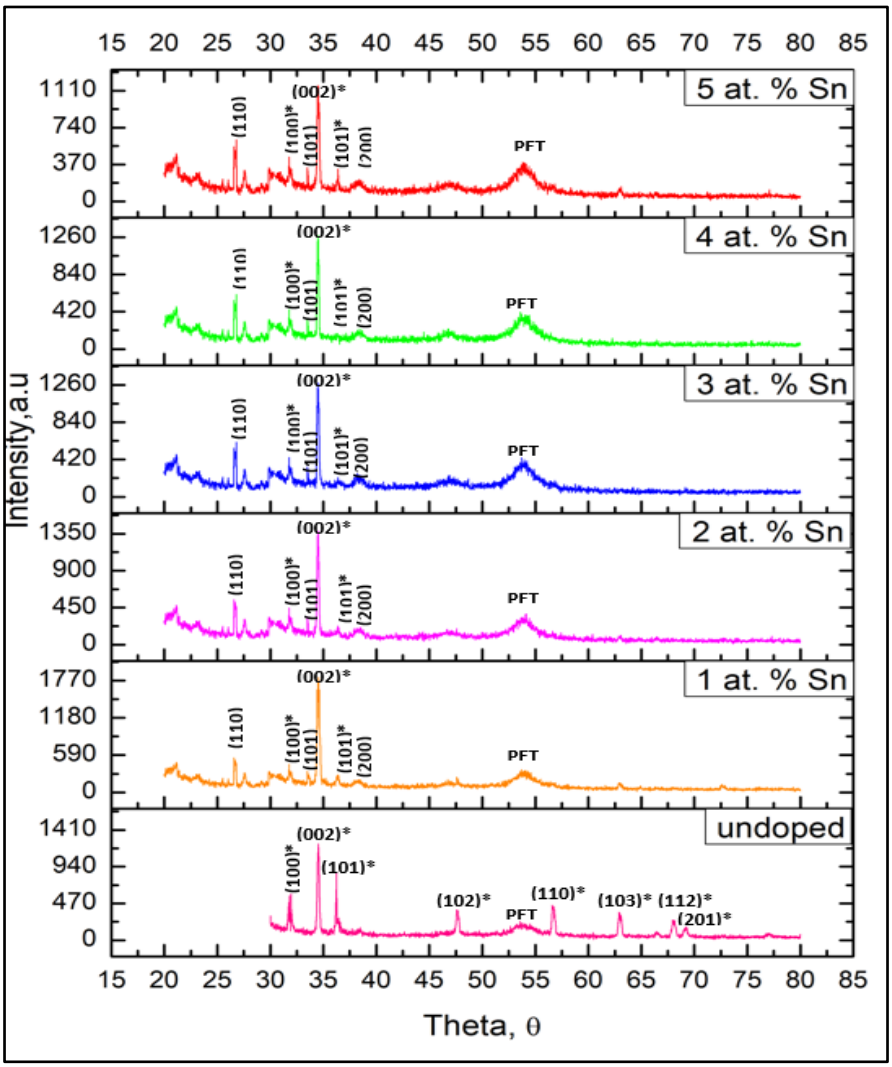

Fig. 2 The XRD spectra at various doping concentrations at.% Sn of (a) undoped, (b) 1 at.%, (c) 2 at.%, (d) 3 at.%, (e) 4 at.%, and (f) 5 at.%

Furthermore, the dominance of this peak indicates that the growth of ZnO nanostructures is strongly oriented along the c-axis, which is favorable for electron transport and humidity-sensing applications [29]. In addition, the presence of multiple well-defined peaks with significant intensities at (a) undoped suggests that the original polycrystalline structure of pure ZnO, as synthesized, has been maintained and remains in a highly crystalline form, as described by Subki et al. [30]. Previous studies, such as Xu et al. [26], have reported similar XRD patterns for Sn-doped ZnO thin films. They suggested that low concentrations of Sn doping, such as 1 at.% Sn can elevate the intensity of the (002) peak, signifying an improvement in the c-axis orientation of ZnO thin films. Nonetheless, when Sn doping exceeds 1 at.% Sn, as depicted in Fig. 4.5, the crystallinity of the (002) peak deteriorates.

This decrease in intensity suggests a degradation in the crystalline structure due to defects introduced in the lattice [30].

Researchers, including Lee and Park [31], have observed that the (002) peak decreases when the Sn-doping concentration exceeds 2 at.% Sn. They proposed that the (002) peak intensity of Sn-doped ZnO thin films is affected by doping concentration and deposition parameters. A similar report from Algün and Akçay [14] stated that the (101) peak intensity increased with Al doping up to 1 mol%. However, it then weakened as the Al concentration exceeded 1 mol%. This observation was attributed to stress induced by the size mismatch between ZnO and Al ions, as well as the accumulation of Al at grain boundaries as the doping concentration increased.

Electrical Properties

Fig. 3 depicts the I-V plot of the ZnO nanostructure at various doping at.% Sn of (a) undoped, (b) 1 at.%, (c) 2 at.%, (d) 3 at.%, (e) 4 at.%, and (f) 5 at.% at RH% values differed from 40 to 90%. Based on Fig. 3, the I values at 5 V, as well as (40%, 90%) of the ZnO nanostructure deposited for various doping concentrations, are provided in Table 2.

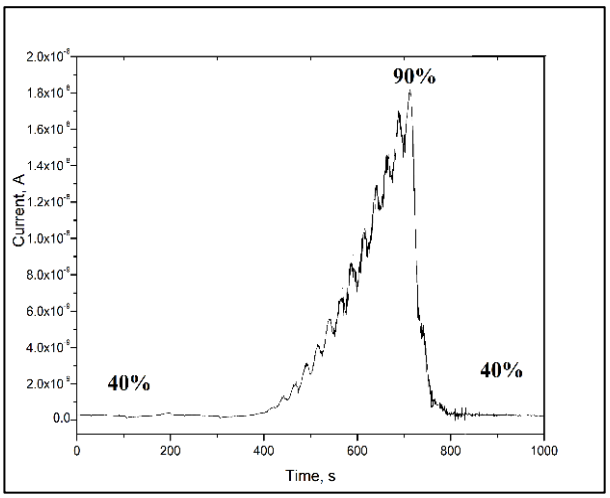

a) undoped

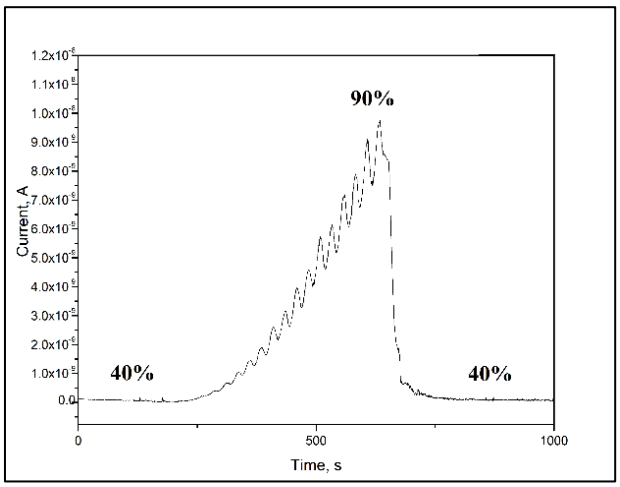

b) 1 at.%

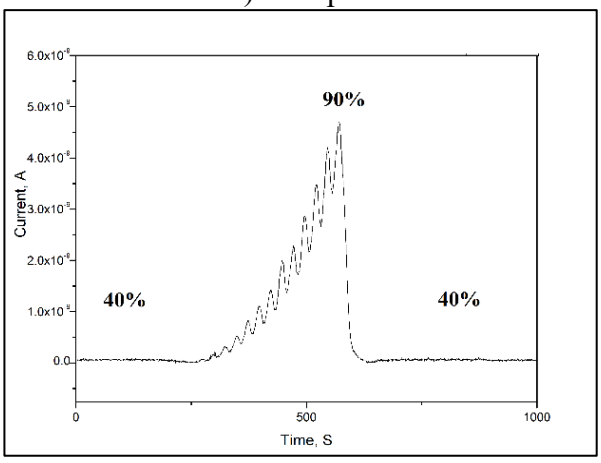

c) 2 at.%

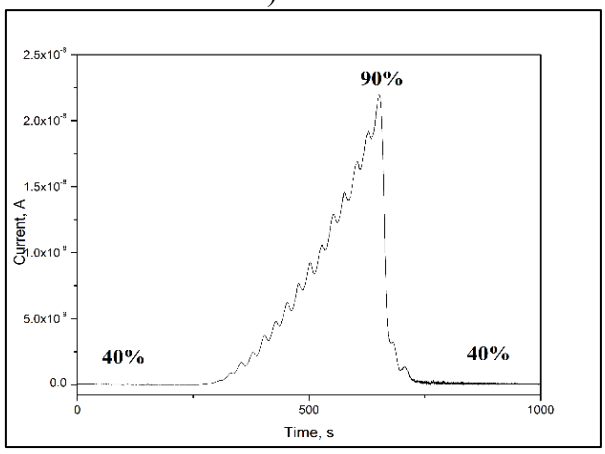

d) 3 at.%

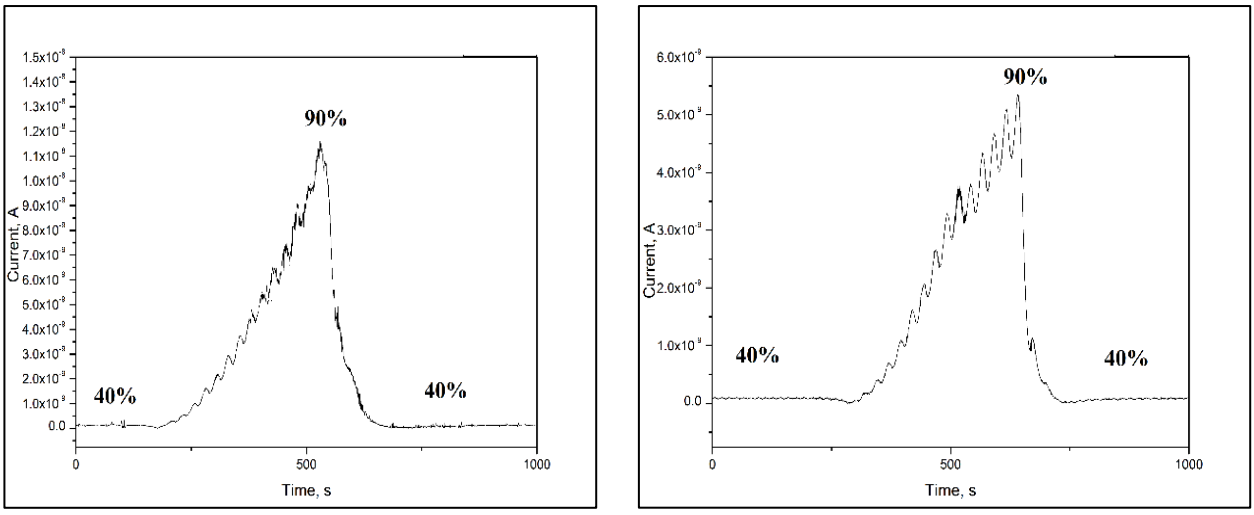

e) 4 at.% f) 5 at.%

Fig. 3 The humidity sensitivity measurements at different doping concentrations at.% Sn of (a) undoped, (b) 1 at.%, (c) 2 at.%, (d) 3 at.%, (e) 4 at.%, and (f) 5 at.% at RH% values ranging from 40 to 90.

The sensitivities of the ZnO nanostructures obtained at different doping concentrations: undoped, 1 at.%, 2 at.%, 3 at.%, 4 at.%, and 5 at.%, respectively, are 79.04, 144.4, 104.2, 98.6, 93.2, and 75.9. During desorption and adsorption processes, the response and recovery times of the ZnO nanostructure-based humidity sensor, deposited with various doping concentrations, are represented in brackets: undoped (231 s, 648 s), 1 at.% (121 s, 411 s), 2 at.% (159 s, 577 s), 3 at.% (294 s, 431 s), 4 at.% (100 s, 177 s), and 5 at.% (149 s, 80 s). The calculated sensitivities, responses, and recovery times are displayed in Table 2 below:

Table 2. Current-Voltage Data and Calculated Sensitivity, Response, and Recovery Times of Sn-Doped ZnO Nanostructures at 5 V

Doping at.% Sn	Current of 5 V (40% RH) [A]	Current of 5 V (90% RH) [A]	Sensitivity	Response time [s]	Recovery time [s]
undoped	1.49×10^{-10}	2.66×10^{-8}	178.5	231	648
1	6.75×10^{-11}	9.75×10^{-9}	144.4	121	411
2	5.56×10^{-11}	4.52×10^{-9}	104.2	186	577
3	2.22×10^{-10}	2.19×10^{-8}	98.6	294	431
4	1.23×10^{-10}	1.15×10^{-8}	93.2	100	177
5	7.05×10^{-11}	5.35×10^{-9}	75.9	149	80

Sensitivity declines when the Sn dopant at% is increased beyond an optimal level. This behavior is consistent with the literature (e.g., Shishiyanu et al. [32] for NO_2 sensing, and other work on ethanol sensing with Sn-ZnO [33], where at moderate Sn content, sensitivity increases. However, further Sn addition leads to decreased performance. The likely reasons are that excessive Sn leads to defect clustering or secondary phase formation, reduces the number of available adsorption sites, and increases charge-carrier recombination due to trap states [34].

Based on Table 2, the sensitivity trend revealed a general decrease as the doping concentration increased, with 1 at.% Sn demonstrating the highest sensitivity (144.4) among the doped samples. Additionally, the sensitivity trend of ZnO nanostructures with varying Sn doping concentrations reveals nonlinear behavior. Although the undoped ZnO sample exhibited the highest sensitivity (178.5), its response time (231 s) and recovery time (648 s) were significantly slower. This indicates that, while oxygen vacancies in undoped ZnO promote high water adsorption, limited charge transport and greater hysteresis hinder fast desorption, resulting in sluggish sensor dynamics. Hence, high sensitivity alone does not guarantee practical sensing performance.

In contrast, the 1 at.% Sn-doped ZnO nanostructure demonstrated an optimal balance between sensitivity (144.4) and much faster response (121 s) and recovery (411 s). This improvement can be attributed to the substitutional incorporation of Sn^{4+} ions into the Zn^{2+} lattice sites. Meanwhile, the smaller ionic radius of Sn^{4+} (0.69 Å) compared to Zn^{2+} (0.74 Å) induces a slight lattice strain that enhances c-axis orientation, reduces defect scattering, and promotes better crystallinity. In essence, these structural modifications improve carrier mobility, thereby accelerating electron-hole exchange and enabling faster sensor response.

However, when the Sn doping concentration exceeded 1 at.%, the crystallinity and sensitivity progressively deteriorated. At higher doping levels (≥ 2 at.% Sn), the excessive substitution of Zn^{2+} with Sn^{4+} creates significant lattice mismatch, strain, and dislocations. These structural defects act as charge trapping centers, disrupting the conduction pathway and reducing the density of active adsorption sites. Consequently, the sensitivity decreases with increasing Sn concentration. Similar observations have been reported in previous studies, where excessive dopant incorporation led to lattice distortion and defect-induced degradation of ZnO's electrical and sensing performance [35].

Overall, these results demonstrate that the sensing behavior is governed by a trade-off between high sensitivity and fast response/recovery times. At the same time, undoped ZnO provides higher sensitivity due to abundant oxygen vacancies, controlled doping at 1 at.% Sn optimizes the structural and electronic properties, resulting in a more reliable and practical humidity sensor.

Conclusion

This study demonstrates a strong correlation among Sn doping concentration, structural evolution, and humidity-sensing performance of ZnO nanostructures deposited on AZO/PET substrates via the sol-gel immersion method. Specifically, XRD analysis confirmed that undoped ZnO possessed good crystallinity, yet the incorporation of 1 at.% Sn further enhanced the (002) orientation and long-range structural order due to the slight lattice strain introduced by substitutional Sn^{4+} ions. At higher Sn concentrations (>1 at.%), excessive dopant incorporation led to lattice distortion, dislocations, and oxygen vacancy-related defects, disrupting the crystal structure and reducing crystallinity.

These structural changes were reflected in the sensing properties. Although undoped ZnO yielded the highest sensitivity (178.5), its slow response (231 s) and recovery (648 s) times restrict its practical use. In comparison, 1 at.% Sn-doped ZnO achieved a balanced performance, combining high sensitivity (144.4) with significantly faster response (121 s) and recovery (411 s). This demonstrates that controlled doping provides a better trade-off between accuracy and speed, making 1 at.% Sn the optimal concentration.

The practical implication of these findings is that low-level Sn doping enables the fabrication of flexible humidity sensors with improved response speed and stability, which are crucial for real-time monitoring in environmental, industrial, and biomedical applications. For future work, it is recommended to evaluate the long-term stability of the sensors under continuous operation, assess their performance under mechanical bending or stretching to confirm durability for flexible electronics, and explore integration into wearable and portable monitoring systems. Nevertheless, these studies will be essential to fully establish the applicability of Sn-doped ZnO nanostructures in next-generation flexible sensing devices.

Acknowledgment

The authors extend their profound appreciation to the members of the NANO-ElecTronic Center (NET) for their invaluable assistance, and to the Research Management Center (RMC), Universiti Teknologi MARA (UiTM), as well as the Ministry of Higher Education (MOHE) for the provision of financial support

References

[1] C. Dubey, B. Kumar, Organic humidity sensors with different materials and its application in environment monitoring, in: 2018 5th IEEE Uttar Pradesh Section International Conference on Electrical, Electronics and Computer Engineering (UPCON), IEEE, 2018, pp. 1–6.

[2] F. Li, P. Li, H. Zhang, Preparation and research of a high-performance ZnO/SnO_2 humidity sensor, Sensors. 22 (1) (2022).

[3] B.C. Anand, R. Shashidhar, N. Choudhary, Application of SRCBD S: SnO_2 nanostructured thin films as room temperature gas and humidity sensors, J. Korean Phys. Soc. 82 (4) (2023) 392–410.

[4] S. Yu, H. Zhang, C. Chen, C. Lin, Investigation of humidity sensor based on Au modified ZnO nanosheets via hydrothermal method and first principle, Sens. Actuators B Chem. 287 (2019) 526-534.

[5] X.T.Y. Gu, Z. Ye, N. Sun, X. Kuang, W. Liu, X. Song, L. Zhang, W. Bai, Preparation and properties of humidity sensor based on K-doped ZnO nanostructure, J. Mater. Sci. Mater. Electron. 30 (20) (2019) 18767–18779.

[6] C.-C. Chou, L.-H. Shih, S.-J. Chang, The study of humidity sensor based on Li-doped ZnO nanorods by hydrothermal method, Microsyst. Technol. 28 (1) (2022) 423–427.

[7] R.C.H. Li, B. Meng, H. Jia, D. Wang, Z. Wei, R. Li, Optical humidity sensor based on ZnO nanomaterials, in: 2020 IEEE 5th Optoelectronics Global Conference (OGC), IEEE, 2020, pp. 169–172.

[8] R.M. Akhir, W.M.W. Harrum, I. Buniyamin, M. Rusop, Z. Khusaimi, Enhanced structural and morphological properties of ZnO nanorods using plant extract-assisted solution immersion method, Mater. Today Proc. 48 (2022) 1855–1860.

[9] J. Soudi, S.K.M., S.B.K., P.S. Patil, S.R. Maidur, B.K.M., Thermo-optic effects mediated self-focusing mechanism and optical power limiting studies of ZnO thin films deposited on ITO coated PET substrates by RF magnetron sputtering under continuous wave laser regime, Optik (Stuttg.) 225 (2021) 165835.

[10] R.S.M.V. Arularasu, R. Vignesh, T.V. Rajendran, PVDF/ZnO hybrid nanocomposite applied as a resistive humidity sensor, Surf. Interfaces 21 (2020) 100780.

[11] M. Bai, M. Chen, X. Li, Q. Wang, One-step CVD growth of ZnO nanorod/SnO_2 film heterojunction for NO_2 gas sensor, Sens. Actuators B Chem. 373 (2022).

[12] L. Niu, S. Hong, M. Wang, Properties of ZnO with oxygen vacancies and its application in humidity sensor, J. Electron. Mater. 50 (8) (2021) 4480–4487.

[13] L.A.N. Üzar, G. Algün, N. Akçay, D. Akcan, Structural, optical, electrical and humidity sensing properties of (Y/Al) co-doped ZnO thin films, J. Mater. Sci. Mater. Electron. 28 (16) (2017) 11861–11870.

[14] G. Algün, N. Akçay, Enhanced sensing characteristics of relative humidity sensors based on Al and F co-doped ZnO nanostructured thin films, J. Mater. Sci. Mater. Electron. 30 (17) (2019) 16124–16134.

[15] D. Brzezińska, D. Bochenek, M. Zubko, P. Niemiec, I. Matuła, Properties of Sn-doped PBZT ferroelectric ceramics sintered by hot-pressing method, Mater. 17 (20) (2024).

[16] R. Brahem, H. Rahmouni, N. Farhat, J. Dhahri, K. Khirouni, L.C. Costa, Electrical properties of Sn-doped $Ba_{0.75}Sr_{0.25}Ti_{0.95}O_3$ perovskite, Ceram. Int. 40 (7A) (2014) 9355–9360.

[17] T. Habeeb, A. Almalki, A.H. Bashal, Synthesis, structural modification, and dielectric property enhancement of manganese and tin-doped bentonite composites for high-performance energy storage applications, Arab. J. Chem. 18 (2024) 2012024.

[18] T. Tamai, M. Watanabe, Y. Kobayashi, Y. Nakahara, S. Yajima, Surface modification of PEN and PET substrates by plasma treatment and layer-by-layer assembly of polyelectrolyte multilayer thin films and their application in electroless deposition, RSC Adv. 7 (53) (2017) 33155–33161.

[19] K. Lazarova, S. Bozhilova, S. Ivanova, D. Christova, T. Babeva, Flexible and transparent polymer-based optical humidity sensor, Sensors 21 (11) (2021).

[20] H. Yan, Z. Chen, L. Zeng, Z. Wang, G. Zheng, R. Zhou, The effect of rGO-doping on the performance of SnO_2/rGO flexible humidity sensor, Nanomaterials 11 (12) (2021).

[21] N. Parimon, et al., Annealing temperature dependency of structural, optical and electrical characteristics of manganese-doped nickel oxide nanosheet array films for humidity sensing applications, Nanomater. Nanotechnol. 11 (2021) 1847980420982788.

[22] A.S. Ismail, M.H. Mamat, M.M. Yusoff, M.F. Malek, A.S. Zoolfakar, R.A. Rani, A.B. Suriani, A. Mohamed, M.K. Ahmad, M. Rusop, Enhanced humidity sensing performance using Sn-doped ZnO nanorod array/SnO_2 nanowire heteronetwork fabricated via two-step solution immersion, Mater. Lett. 210 (2018) 258–262.

[23] M.R.A.S. Ismail, M.H. Mamat, I.B. Shameem Banu, R. Amiruddin, M.F. Malek, N. Parimon, A.S. Zoolfakar, N.D. Md. Sin, A.B. Suriani, M.K. Ahmad, Structural modification of ZnO nanorod array through Fe-doping: Ramification on UV and humidity sensing properties, Nano-Struct. Nano-Objects 18 (2019) 100262.

[24] N.A.M. Asib, M.H. Mamat, M. Rusop, Z. Khusaimi, Investigation on properties of ZnO nanorods grown at different immersion time on TiO_2 seed layer, AIP Conf. Proc. 2151 (1) (2019) 020015.

[25] A.S. Ismail, M.H. Mamat, M.F. Malek, S.A. Saidi, M.M. Yusoff, R. Mohamed, N.D. Md. Sin, A.B. Suriani, M. Rusop, Structural, optical, and electrical properties of Ni-doped ZnO nanorod arrays prepared via sonicated sol–gel immersion method, AIP Conf. Proc. 1963 (1) (2018) 020029.

[26] L. Xu, G. Zheng, F. Xian, J. Su, The morphological evolution of ZnO thin films by Sn ions doping and its influence on the surface energy and photocatalytic activity, Mater. Chem. Phys. 229 (2019) 215–225.

[27] H. Wang, R. Bhattacharjee, I.-M. Hung, L. Li, R. Zeng, Material characteristics and electrochemical performance of Sn-doped ZnO spherical-particle photoanode for dye-sensitized solar cells, Electrochim. Acta 111 (2013) 797–801.

[28] I. Saurdi, M.H. Mamat, M.F. Malek, M. Rusop, Preparation of aligned ZnO nanorod arrays on Sn-doped ZnO thin films by sonicated sol–gel immersion fabricated for dye-sensitized solar cell, Adv. Mater. Sci. Eng. 2014 (2014) 636725.

[29] G. Algün, M. Alshater, N. Akçay, Improved humidity sensing performances of boron doped ZnO nanostructured thin films depending on boron concentration, Phys. Scr. 99 (5) (2024).

[30] M.D.B., M.R.M.A. Shamsul Rahimi A. Subki, M.H. Mamat, M.M. Zahidi, M.H. Abdullah, B. Shameem Banu, N. Vasimalai, M.K. Ahmad, N. Nayan, S.A. Bakar, A. Mohamed, Optimization of aluminum dopant amalgamation immersion time on structural, electrical, and humidity-sensing attributes of pristine ZnO for flexible humidity sensor application, Chemosensors 10 (11) (2022).

[31] J.-H. Lee, B.-O. Park, Transparent conducting ZnO:Al, In and Sn thin films deposited by the sol–gel method, Thin Solid Films 426 (1) (2003) 94–99.

[32] S.T. Shishiyanu, T.S. Shishiyanu, O.I. Lupan, Sensing characteristics of tin-doped ZnO thin films as NO_2 gas sensor, Sens. Actuators B Chem. 107 (1) (2005) 379–386.

[33] P. Zhang, G. Pan, B. Zhang, J. Zhen, Y. Sun, High sensitivity ethanol gas sensor based on Sn-doped ZnO under visible light irradiation at low temperature, Mater. Res. 17 (2014) 817–822.

[34] Z. Feng, A. Gaiardo, M. Valt, B. Fabbri, D. Casotti, S. Krik, L. Vanzetti, M. Della Ciana, S. Fioravanti, S. Caramori, V. Guidi, Investigation on sensing performance of highly doped Sb/SnO_2, Sensors 22 (3) (2022).

[35] N. Munna, R. Abdur, S.F.U. Farhad, R. Islam, M.S. Bashar, M. Kamruzzaman, S. Aziz, M.A.A. Shaikh, M. Hossain, M.S. Jamal, Influence of Sn doping on the optoelectronic properties of ZnO nanoparticles, Nanoscale Adv. 5 (18) (2023) 4996–5004.